

Simulation of a Liquid Scintillator Off-axis Detector

Peter Litchfield, Leon Mualem, David Petyt

Introduction

Off-axis-NOTE-SIM-23 described the generation and analysis of data from a solid scintillator off-axis detector at a site 735km from Fermilab. This note describes an analysis of the liquid scintillator detector that is featured in the off-axis proposal both at 735km, to compare with the solid scintillator detector, and at 820km, which is the favored site in the proposal.

The earlier note assumed a Δm^2 of 0.0025 eV^2 . Numbers will also be given here for the 820km site with $\Delta m^2=0.0020 \text{ eV}^2$, the present Super-K best fit point.

The procedure was very similar to that of the solid analysis. This short note will just detail the differences.

Neutrino Event Generator

The solid analysis generated events using NEUGEN2. This analysis used the latest version of NEUGEN, NEUGEN3 which supercedes the previous versions. The most important changes are the inclusion of coherent pion production according to the model by Rein and Seghal, modifications to the resonance model to restrict unphysical event generation at high W, improved treatment of the kinematic regime of resonance and DIS overlap, and improved treatment of DIS hadronization into specific exclusive final states, and inclusion of formation zone effects in the simulation of the intranuclear hadronic cascade. In addition the NEUGEN2 analyses did not have the intra-nuclear cascade code INTRANUKE implemented and thus there was no nuclear absorption. The current generation included the nuclear absorption.

These quite extensive changes to the generated final states make it difficult to compare details of the distributions with the solid analysis but the improved physics and background simulations make it important to use the most up-to-date formulation.

Detector Definition

The detector simulated is that described in the draft proposal. The passive absorber is identical to that simulated for the solid scintillator case. The active elements are PVC extrusions 14.6m in length, 1.22m wide and 0.029m thick containing 30 cells 3.96cm in width transverse to the beam and 2.6cm deep in the beam direction. The external walls of the extrusion are 1.5mm thick and the internal walls between cells are 1.0mm thick. The readout and photodetector simulation is identical to that for the solid scintillator. The light output was again adjusted such that a minimum ionizing particle at the far end of a strip produced a mean of 35 detected phototelectrons.

Event Generation and Analysis

The event generation and reconstruction was done identically to that for the solid scintillator. A training sample of 1.4M events and a similar sized test sample were generated. The ν_μ CC, ν_e CC and NC events were generated flat in energy over two energy ranges, 0.15 GeV to 3 GeV and 3 GeV to 20 GeV with equal numbers of events in each sub-sample.

The main analysis used the same event parameters as the solid scintillator analysis. The parameter distributions were very similar and are shown in Figures 1 to 10. The main differences were a slight increase in the number hits per plane and a flattening of the Hough hit fraction distribution for the ν_e CC events. Compare Figure 1 of this note with Figure 8 of the solid scintillator note. The former effect is probably attributable to the increase in thickness of the scintillator cells in the beam direction. This gives a greater probability that a single particle makes hits in more than one cell. The Hough filter parameters were adjusted to include more of the event hits in the Hough track and reproduce the ν_e solid scintillator distribution. However this also increased the fraction of hits in the other event types and the same parameters as in the solid analysis proved optimum. The flattening of the Hough hit fraction may also be due to the increased number of hits per

plane but the changes in the hadronic simulations will also affect this distribution.

The beam spectrum and oscillation effects are produced independently of the generation by weighting the generated events. Three cases of beam and oscillation parameters have been studied.

1. The 735 km from Fermilab, 10 km off axis beam and $\Delta m^2=0.0025 \text{ eV}^2$, as used for the solid scintillator analysis.
2. An 820km from Fermilab, 12 km off axis beam and $\Delta m^2=0.0025 \text{ eV}^2$, corresponding to the preferred Ash River site in the proposal.
3. An 820km from Fermilab, 12 km off axis beam and $\Delta m^2=0.0020 \text{ eV}^2$, corresponding to the preferred Ash River site and the latest Super-K best fit parameters.

Selection of ν_e CC events at 730km

The selection process was very similar and used the same variables as the solid analysis. After optimization on the figure of merit the only parameter that it was found necessary to change was the cut on the number of Hough hits per plane, which was raised from 1.3 to 1.5. As before the Figure of Merit (FOM) was rather flat in the parameter space. After optimization of the likelihood cuts the final FOM for reasonable changes in the other cut parameters covered a relative small range of 2-3. The parameter values found in the solid analysis were close to optimum and were adopted again (except for the hits/plane parameter). The numbers of events surviving the cuts are shown in Table 1.

Since the coherent pizero reaction is new in NEUGEN3 and is expected to be a significant background, to enable a better comparison with the solid analysis the numbers are given both with and without (in brackets) the coherent pizero events. Up to the likelihood cuts the coherent pizero events affect only the NC events but the likelihood distribution cuts affect all three data sets.

The FOM is 27.1 ± 0.5 , signal 121.9 ± 1.1 events and background 20.2 ± 0.7 for the full analysis and 29.0 ± 0.5 , signal 123.3 ± 1.1 events and background 18.1 ± 0.6 without the coherent pizero events.

Cut	ν_μ CC	NC	beam ν_e	$\nu_\mu \rightarrow \nu_e$ signal
generated events	459714	411081	458913	
Beam weighted	26898	8118.1	540.4	
beam weighted +osc	11095.0	8118.1	540.4	773.4
reconstructed events	10572.6	5009.5	472.3	686.8
fiducial volume	6770.6	4438.9	371.6	599.3
event length	1642.2	2979.4 (2920.8)	154.8	515.1
Total ph	1082.8	834.3 (823.3)	59.3	427.4
Hough fraction	124.8	37.5 (32.5)	20.7	177.1
Hough hits/plane	19.4	26.3 (21.6)	19.8	166.6
Hough beam angle	5.2	19.6 (150)	18.6	154.4
Likelihood	1.7 (1.7)	7.1 (4.8)	11.4 (11.6)	121.9 (123.3)
Statistical error	0.3 (0.3)	0.6 (0.5)	0.1 (0.1)	1.1 (1.1)
Events remaining	44 (42)	359 (213)	17915 (18242)	17915 (18242)

Table 1 Breakdown of the weighted number of events remaining after the successive cuts at 735km. The last row gives the number of unweighted events remaining after all cuts. Note that the generated events totals do not include events that produced no hits in the detector.

The main difference to the solid analysis is that the cut on the Hough hits per plane removes many more signal events and this results in an optimum with less background and less signal. A signal efficiency similar to the solid efficiency can be obtained by relaxing this and the likelihood cuts but it produces a best FOM approximately 2 smaller.

Suggestions and ideas made since the release of the solid analysis motivated examination of a few more variables.

1. The distance between the event vertex and the Hough track vertex, motivated by the possibility that pizeros will convert downstream of the main event vertex.
2. The pulse height in the first few planes after the vertex, motivated by the possibility that the primary electrons have a single track whereas a converted pizero has two electrons and may produce double the pulse height. The best separation of the electron from other events was found to be if the sum of the pulse height in the 2nd to 4th planes was taken. The first plane is presumably contaminated with other hits around the vertex.
3. The number of missing planes in the Hough track, motivated by the possibility that a showering track may have gaps whereas a pion or muon track would not. The biggest gap in the total event was already a component of the solid likelihood.

Although these variables do show significant differences in the raw distributions, after the cuts the differences are not large. The plots for these variables are shown in Figure 11. Inclusion of these variables in the likelihood ratio produced no improvement in the figure of merit. As in the solid analysis we conclude that the likelihood function is saturated and there is no significant further separation available in an analysis of this sophistication.

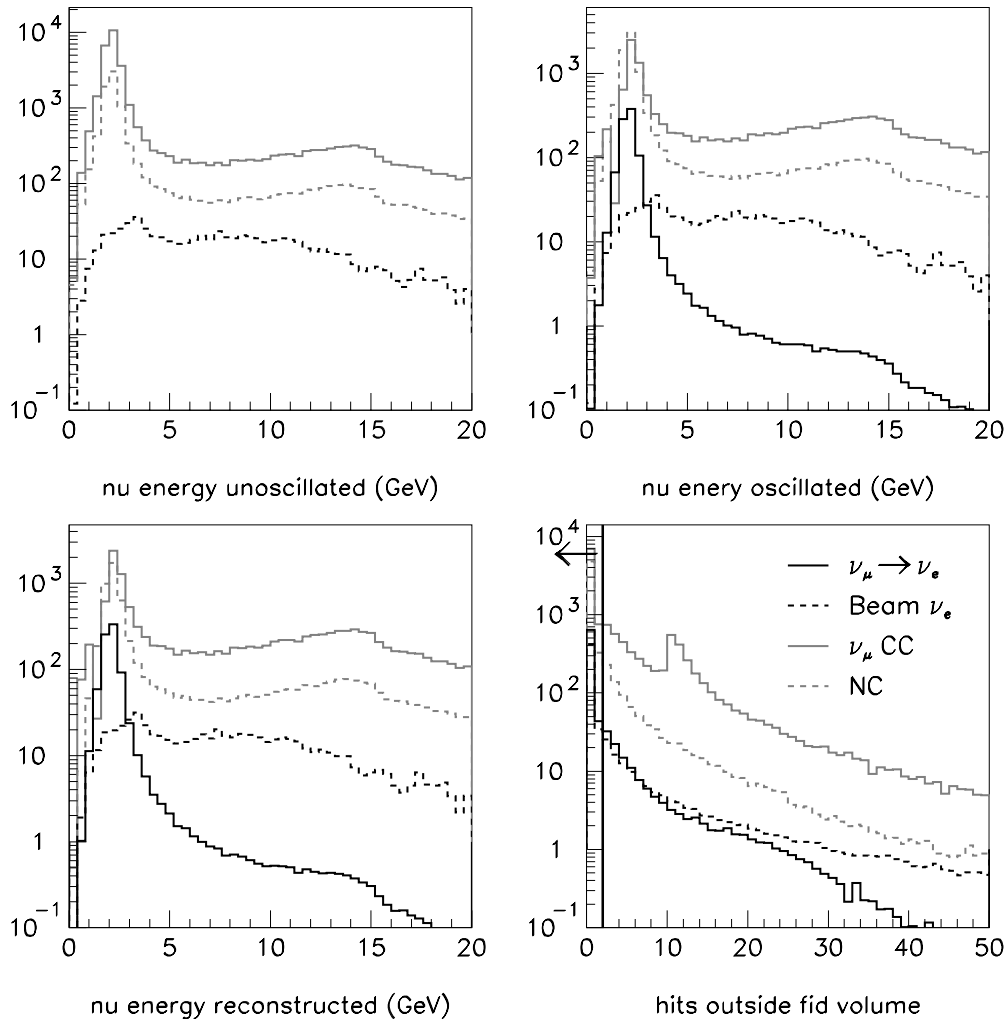


Figure 1 Event samples used in this analysis at 735km. Top left: unoscillated true neutrino energy distributions. Top right: energy distributions after oscillations. Bottom left: energy distributions for events that form a valid cluster. Bottom right: distributions of numbers of hits outside the fiducial volume of the detector. Events with more than 2 hits outside the fiducial volume are rejected.

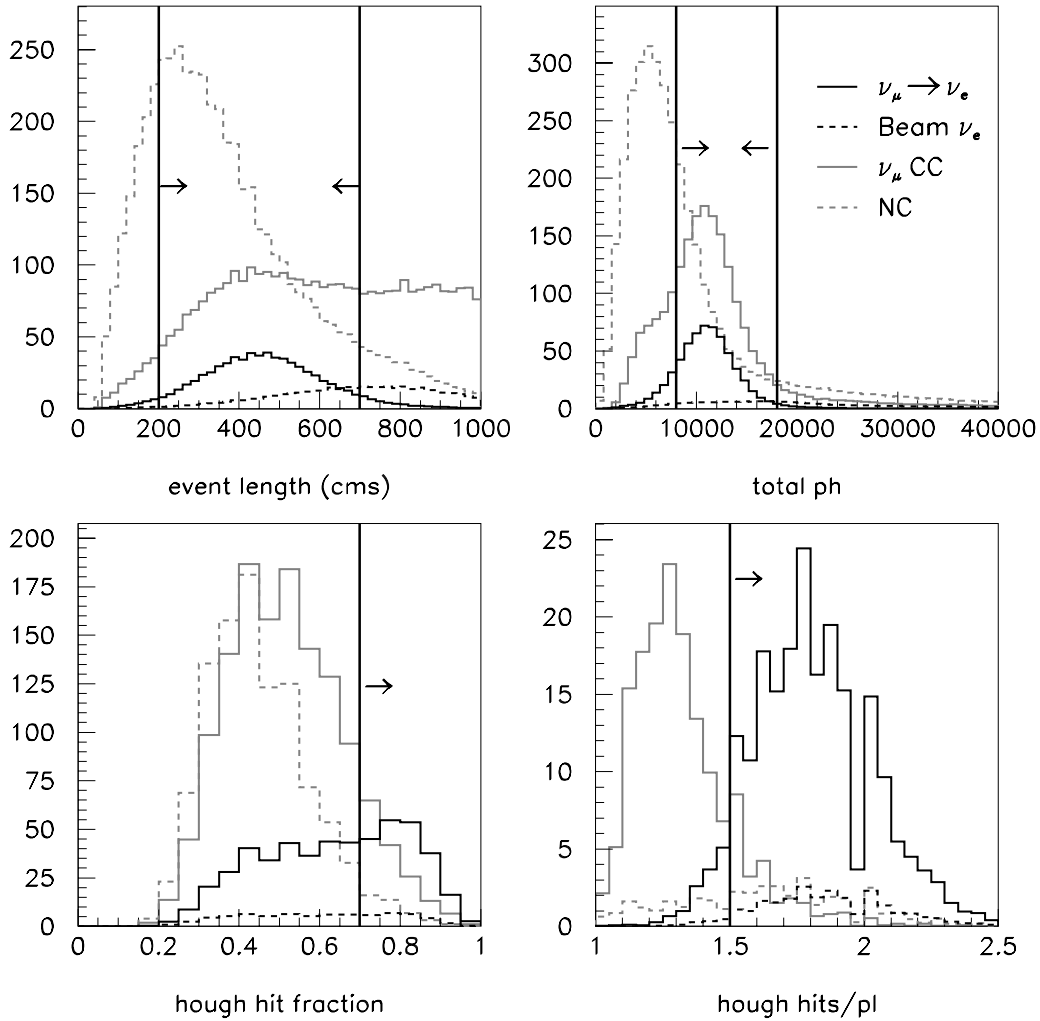


Figure 2 Event distributions used for the cuts at 735km. The vertical lines define the cuts, events on the sides towards which the arrows are pointing pass the cuts. The cuts are performed sequentially in the following order. Top left; event length. Top right; summed pulse height. Bottom left; the fraction of hits in the event found by the Hough Transform filter. Bottom right; the number of hits per plane in the Hough track.

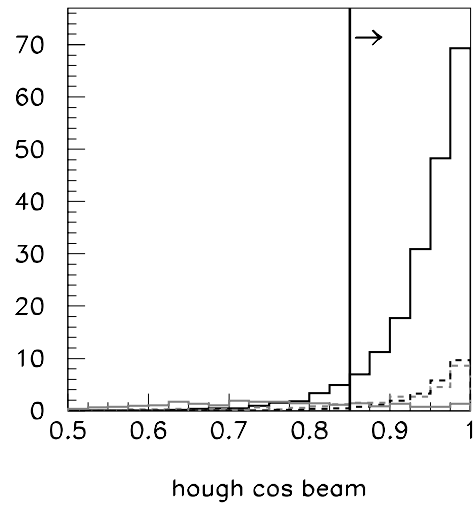


Figure 3 The final cut at 735km; the cosine of the angle between the Hough track direction and the z-axis.

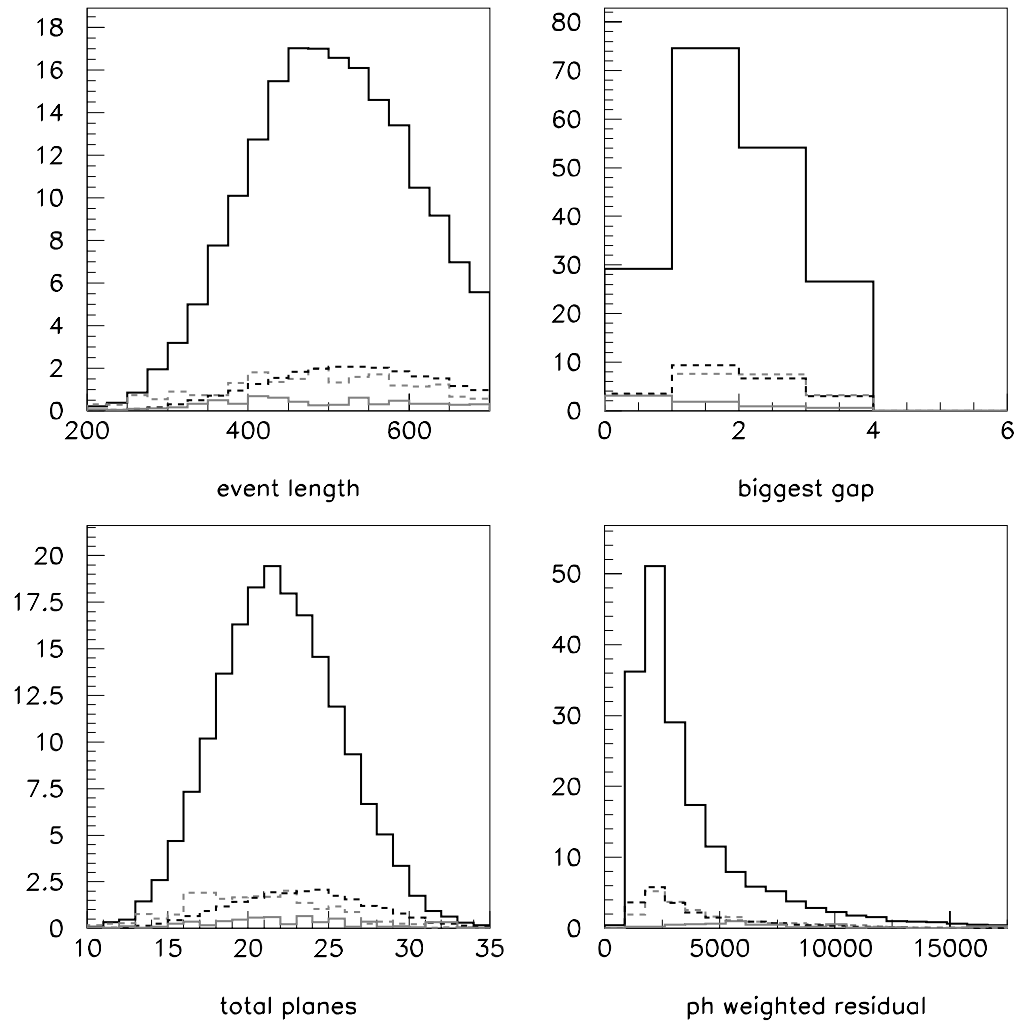


Figure 4 Distributions used in the likelihood function at 735km. Top left; the event length after the cuts. Top right; the largest gap (missed planes) in the event. Bottom left; the total number of hit planes in the event. Bottom right; the pulse height weighted residual to the straight line fitted to the event.

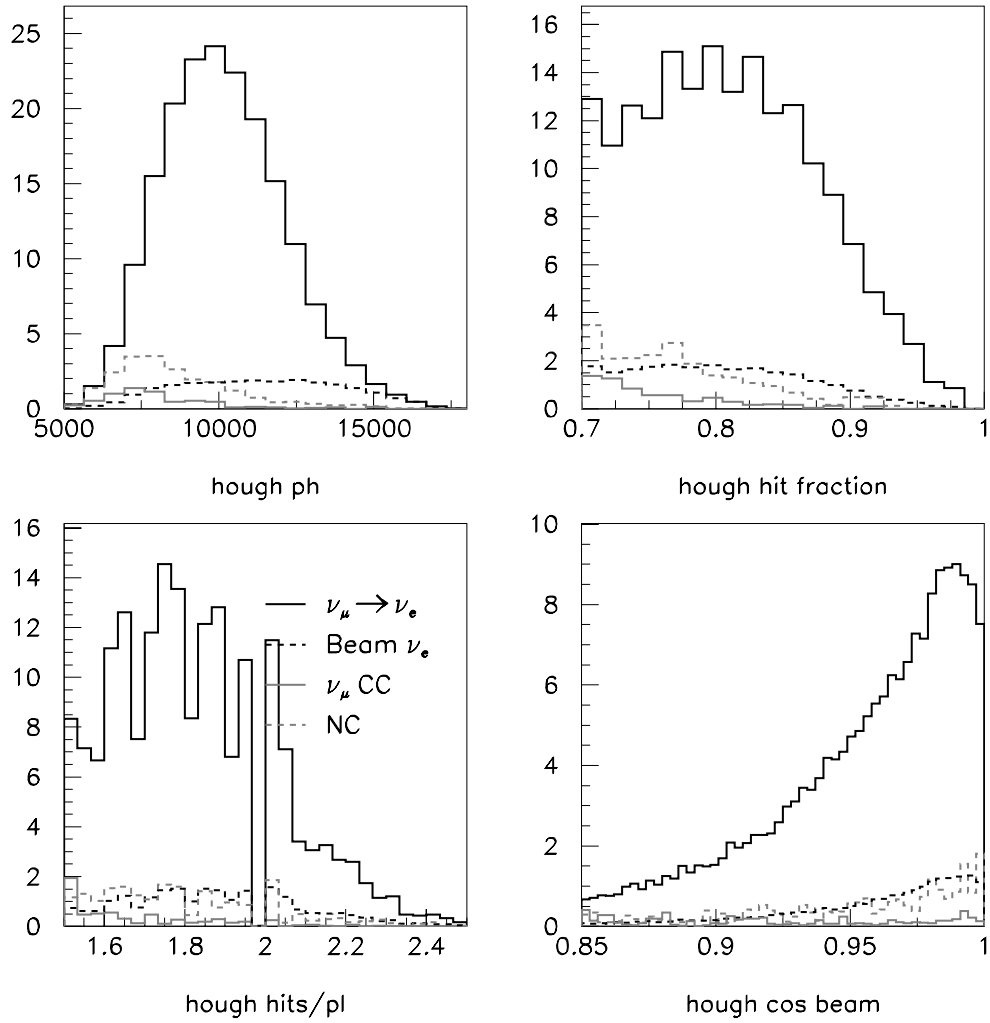


Figure 5 Distributions derived from hits selected by the Hough Transform (HT) filter at 735km. Top left: total pulse height. Top right: fraction of hits selected by the HT filter over the total number of hits in the event. Bottom left: number of hits per plane. Bottom right: cosine of the angle between the straight line fit to the hits and the z axis.

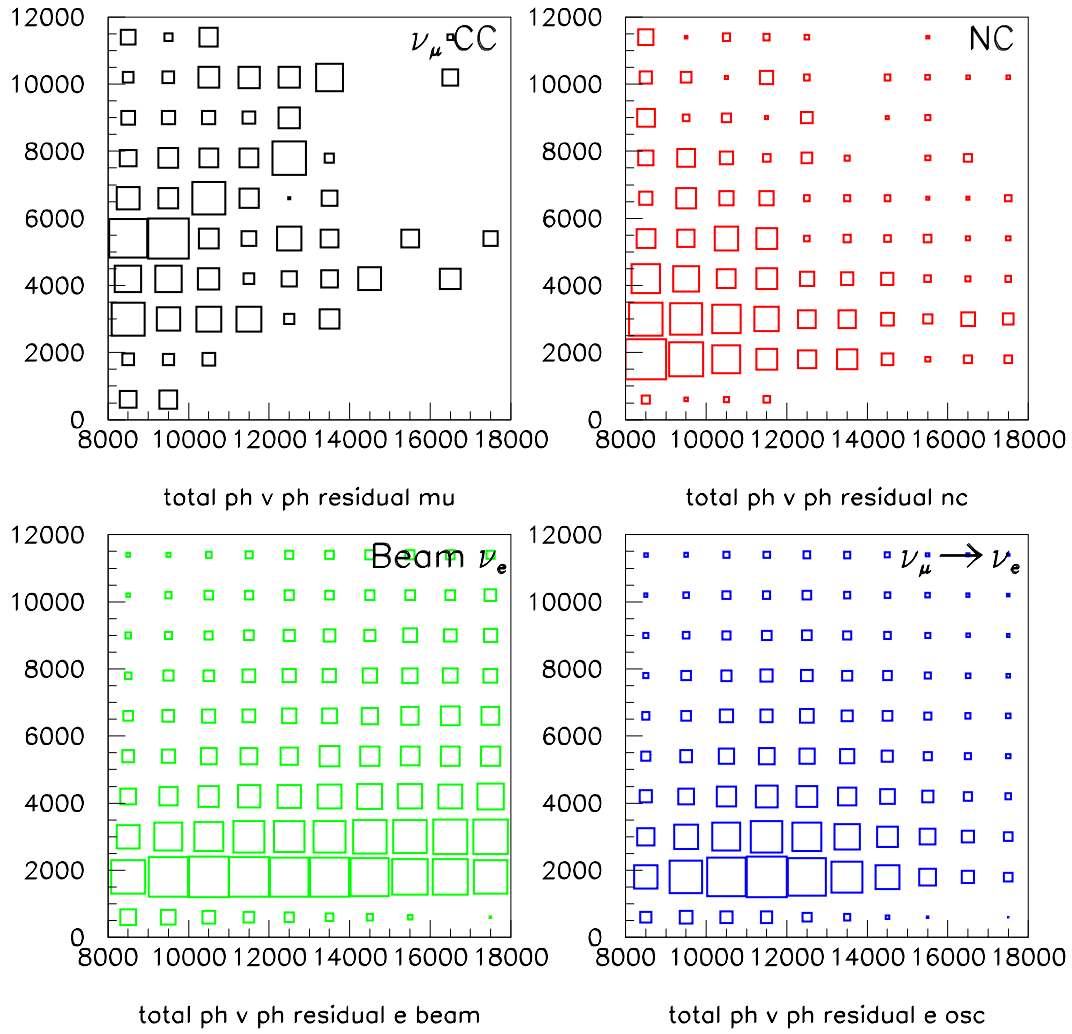


Figure 6 Total pulse height (x) versus pulse height residual (y) distributions for all hits in the four event classes at 735 km.

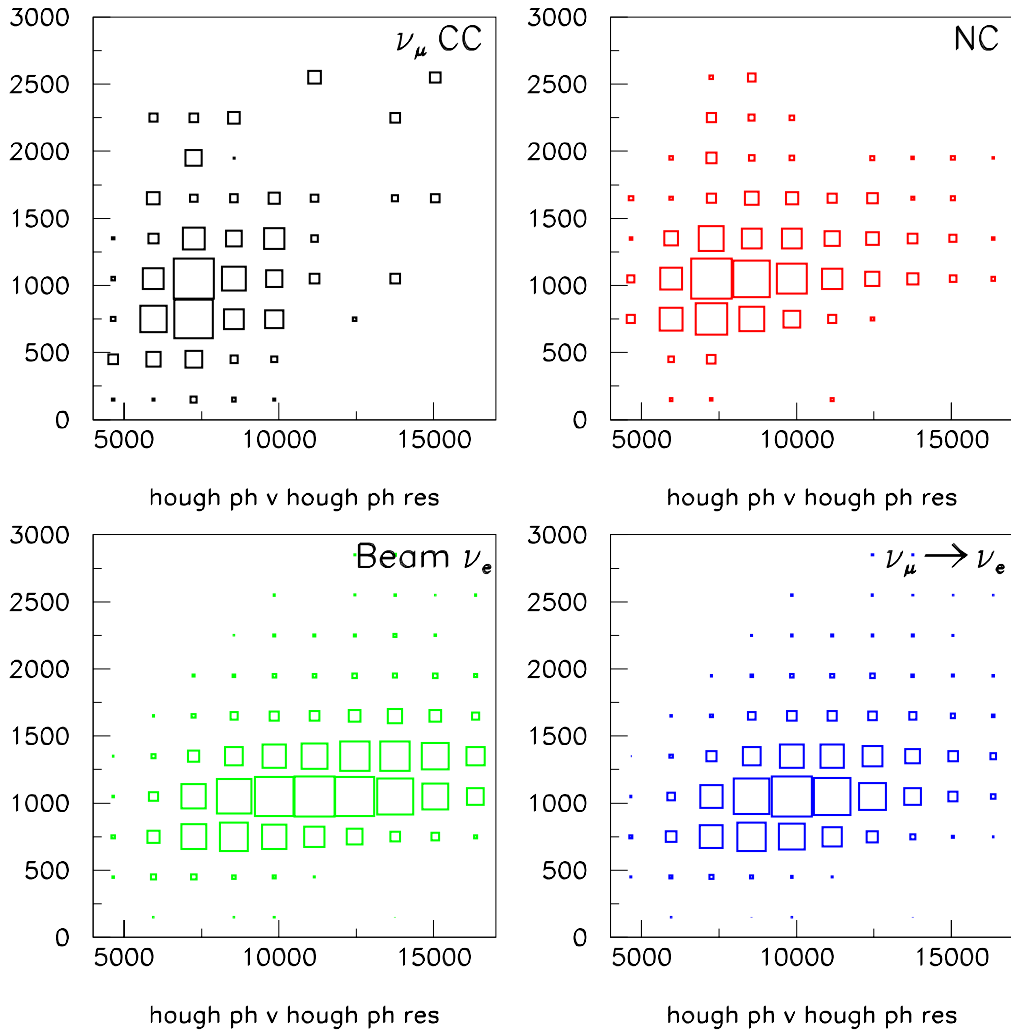


Figure 7 Total pulse height (x) versus pulse height residual (y) distributions from the hits assigned to the Hough track for the four event classes at 735km.

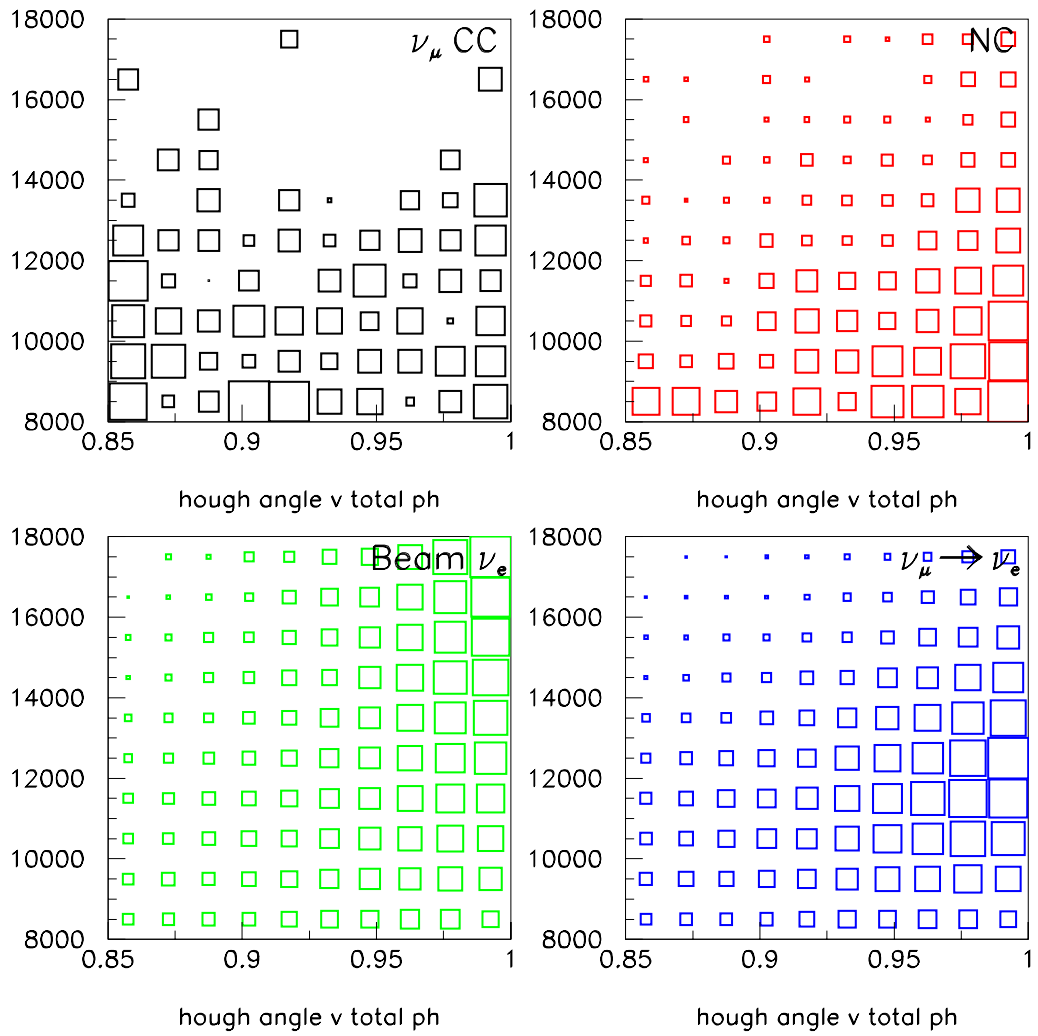


Figure 8 Cosine of the angle between the Hough track and the z axis (x) versus the total pulse height in the event (y) at 735km.

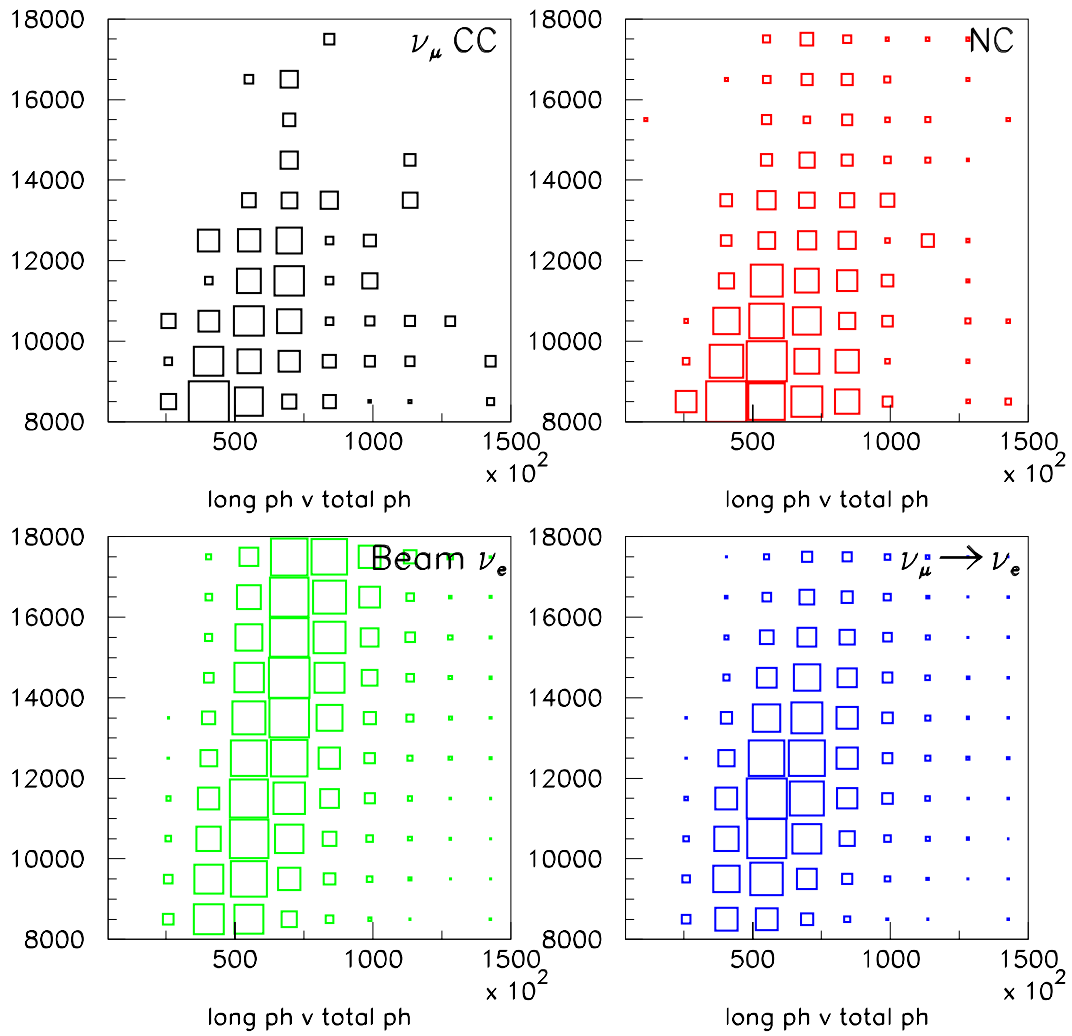


Figure 9 The rms of the pulse height times distance in the z direction (x) versus the total pulse height for hits in the total event (y) at 735km.

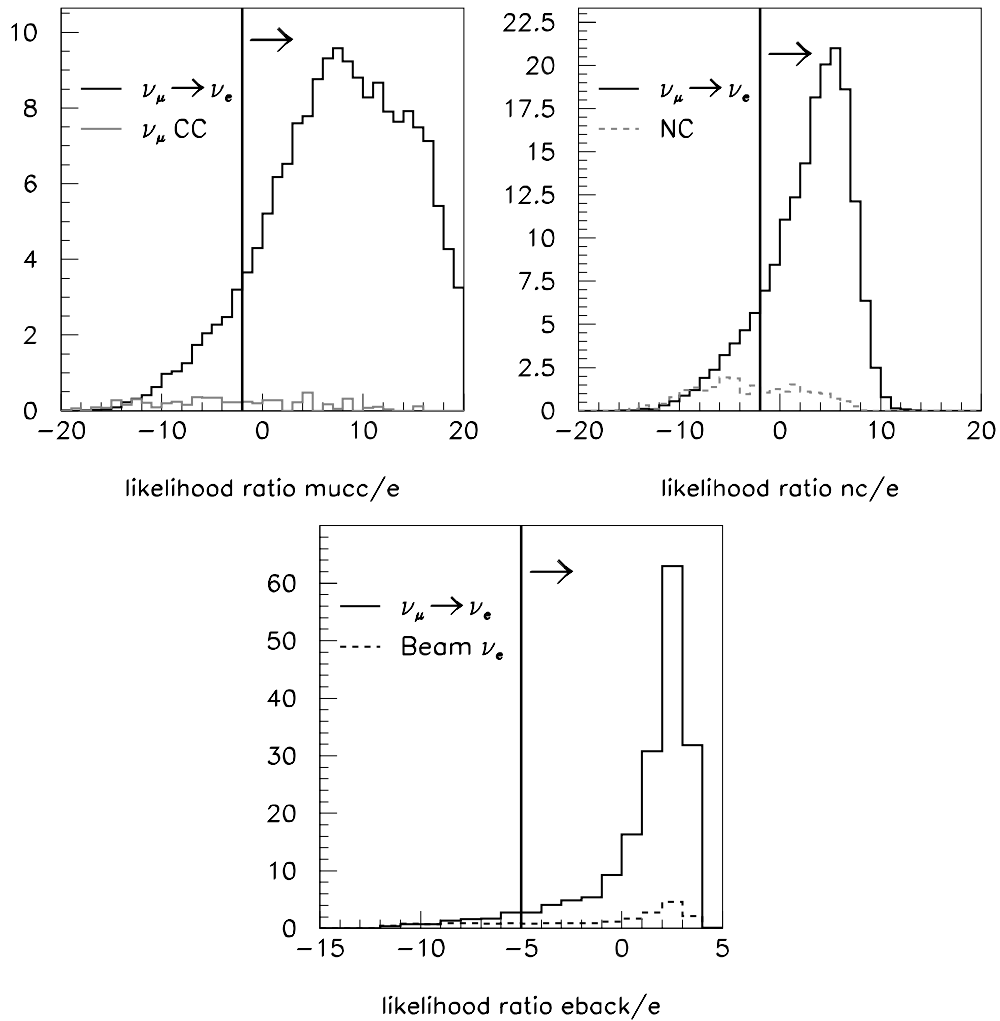


Figure 10 Log likelihood ratio distributions at 735km. Top left; log of the ratio of the ν_μ CC to the oscillated ν_e CC likelihood. Top right; log of the ratio of the NC to the oscillated ν_e CC likelihood. Bottom; log of the ratio of the beam ν_e CC to the oscillated ν_e CC likelihood.

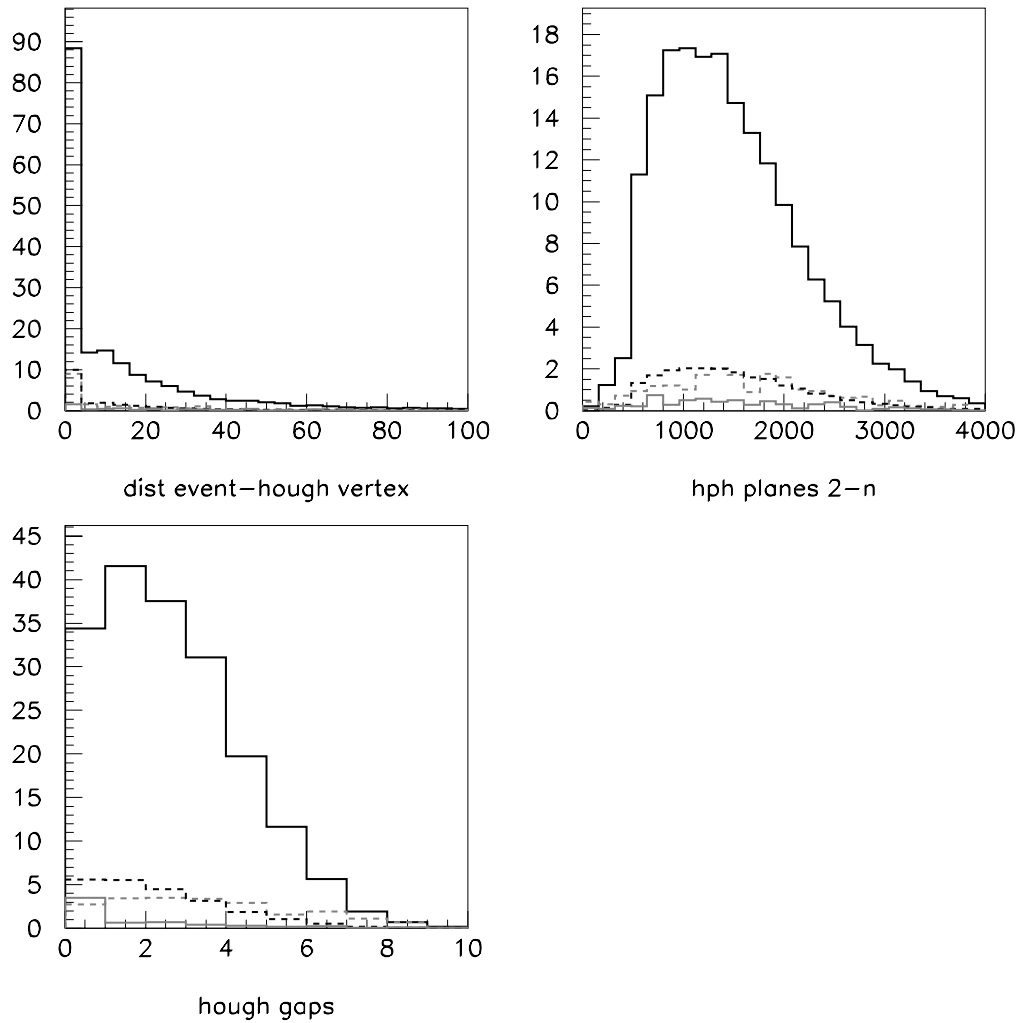


Figure 11 Top left; distance between the event vertex and the Hough track vertex. Top right; summed pulse height in planes 2-4 of the Hough track. Bottom; number of empty planes between the first and last or 20th (whichever comes first) plane of the Hough track.

Selection of ν_e CC events at 820km

Events were weighted to correspond to a detector at 820km from Fermilab, 12km off axis. This was the closest point to the Ash River site for which beam information was available.

The selection parameters were scanned to optimize the FOM but it was found that the parameters for the 735km beam were close to optimum. These same parameters were used in table 2 which repeats table 1 for the 820 km site. The coherent pizero events are included.

Cut	ν_μ CC	NC	beam ν_e	$\nu_\mu \rightarrow \nu_e$ signal
generated events	459714	411081	458913	
Beam weighted	18606.7	5607.3	391.8	
beam weighted +osc	6395.7	5607.3	391.8	596.8
reconstructed events	6078.0	3410.6	342.4	530.4
fiducial volume	3606.8	3019.0	270.3	464.3
event length	739.2	1997.0	114.2	399.5
total ph	354.5	513.3	43.8	322.1
Hough fraction	46.9	23.3	15.5	138.0
Hough hits/plane	7.4	16.5	14.8	128.6
Hough beam angle	1.7	12.2	13.8	117.5
Likelihood	0.6	4.8	7.9	92.4
Statistical error	0.1	0.4	0.1	0.8
Events remaining	49	386	17261	17261

Table 2 Breakdown of the weighted number of events remaining after the successive cuts at 820km. The last row gives the number of unweighted events remaining after all cuts. The raw event sample and the cuts are the same as in Table 1.

The FOM is 25.3 ± 0.4 , the number of signal events 92.4 ± 0.8 and background 13.3 ± 0.4 events. The initial number of oscillated events has been reduced by 177, the final signal by 29 and the background by 7 events. The FOM is reduced by 1.8.

Plots at 820km are in Figures 12-21. Random samples of pictures of selected events for mu CC, e CC and NC are on the web at http://www.physics.umn.edu/~pjl/offaxis/mucc_events_820.ps [ecc_events_820.ps](http://www.physics.umn.edu/~pjl/offaxis/ecc_events_820.ps) and [munc_events_820.ps](http://www.physics.umn.edu/~pjl/offaxis/munc_events_820.ps)

At 820km we have also used a Δm^2 of 0.0020 eV², corresponding to the latest best fit Super-K parameters. Again the best FOM is obtained with the same cut parameters. Table 3 shows the numbers under these conditions.

Cut	ν_μ CC	NC	beam ν_e	$\nu_\mu \rightarrow \nu_e$ signal
generated events	459714	411081	458913	
Beam weighted	18606.7	5607.3	391.8	
beam weighted +osc	8418.4	5607.3	391.8	498.2
reconstructed events	8020.8	3410.6	342.4	442.9
fiducial volume	5198.1	3019.0	270.3	388.8
event length	1348.3	1997.0	114.2	335.3
total ph	891.3	513.3	43.8	262.9
Hough fraction	139.9	23.3	15.5	113.6
Hough hits/plane	20.8	16.5	14.8	105.6
Hough beam angle	4.5	12.2	13.8	96.0
Likelihood	1.5	4.8	7.9	75.6
Statistical error	0.3	0.4	0.1	0.7
Events remaining	52	385	17126	17126

Table 3 Breakdown of the weighted number of events remaining after the successive cuts at 820km with $\Delta m^2=0.0020$ eV². The cuts are the same as for Table 2.

The FOM is 20.1 ± 0.4 , signal 75.6 ± 0.7 events and the background 14.1 ± 0.5 events. It can be seen that the signal goes down and the muon CC background goes up. This detector position may not be optimum for this value of Δm^2 .

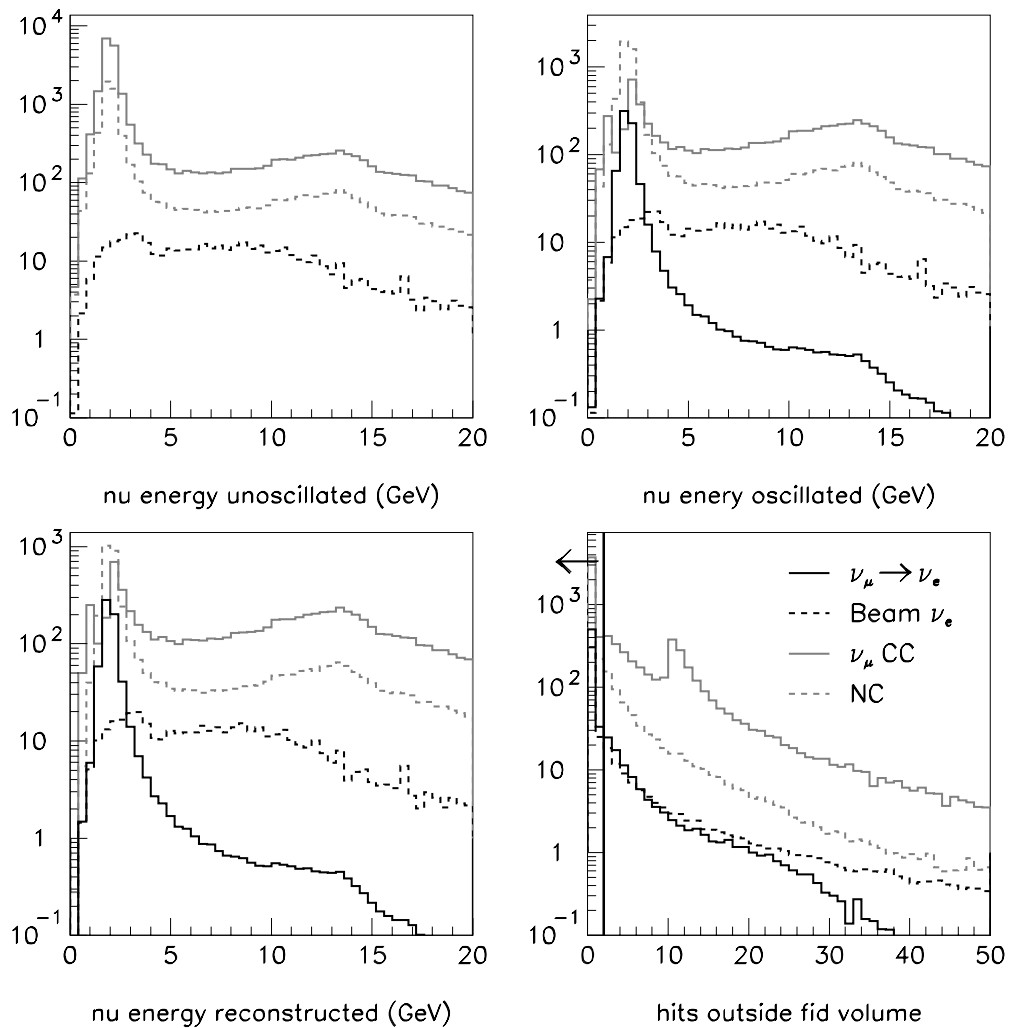


Figure 12 Event samples used in this analysis at 820km. Top left: unoscillated true neutrino energy distributions. Top right: energy distributions after oscillations. Bottom left: energy distributions for events that form a valid cluster. Bottom right: distributions of numbers of hits outside the fiducial volume of the detector. Events with more than 2 hits outside the fiducial volume are rejected.

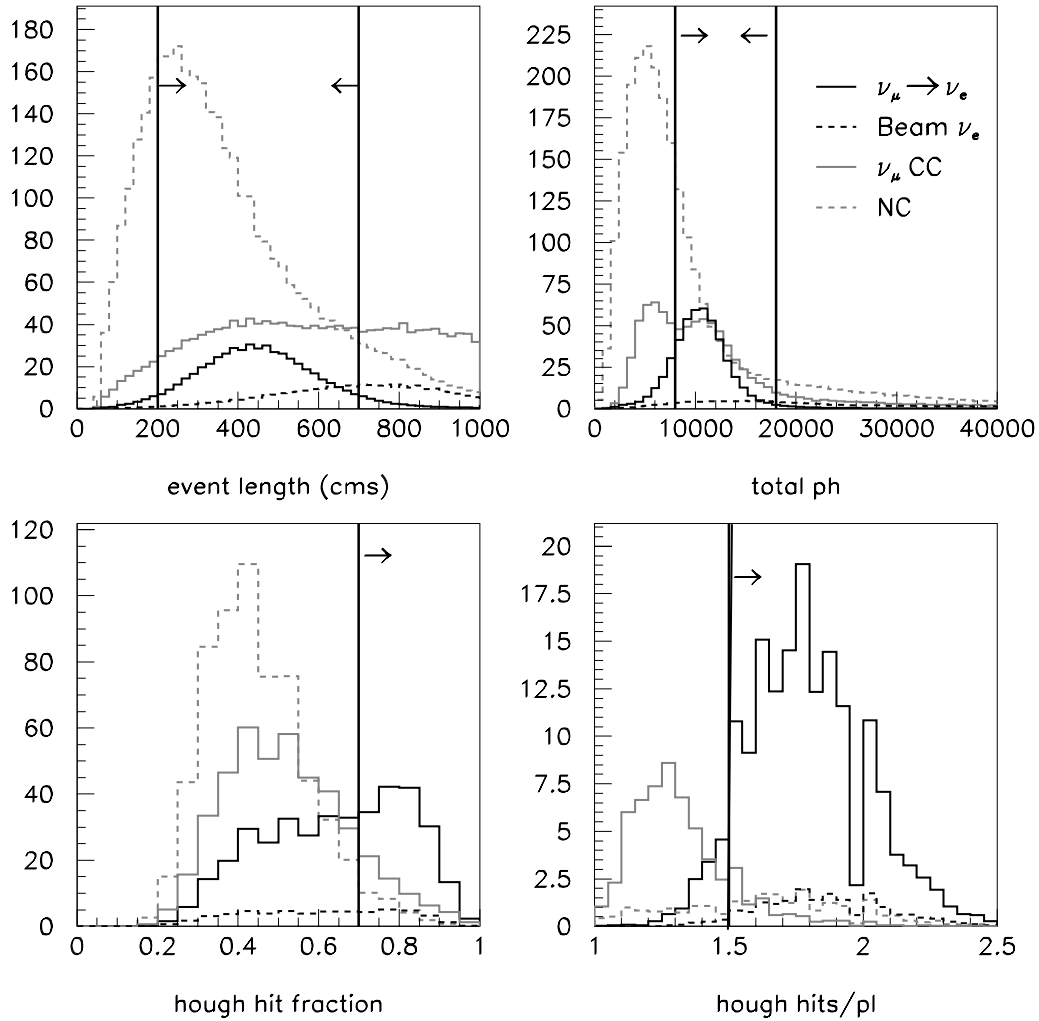


Figure 13 Event distributions used for the cuts at 820km. The vertical lines define the cuts, events on the sides towards which the arrows are pointing pass the cuts. The cuts are performed sequentially in the following order. Top left; event length. Top right; summed pulse height. Bottom left; the fraction of hits in the event found by the Hough Transform filter. Bottom right; the number of hits per plane in the Hough track.

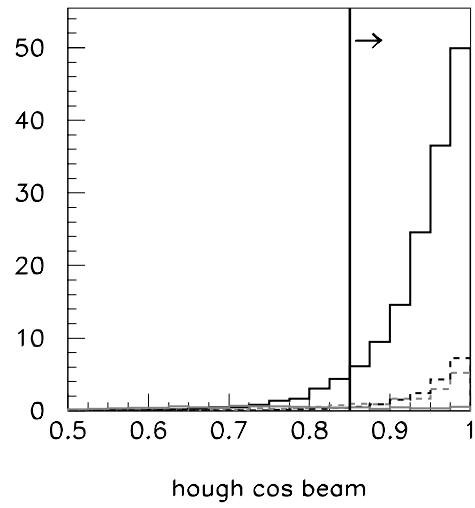


Figure 14 The final cut at 820km; the cosine of the angle between the Hough track direction and the z-axis.

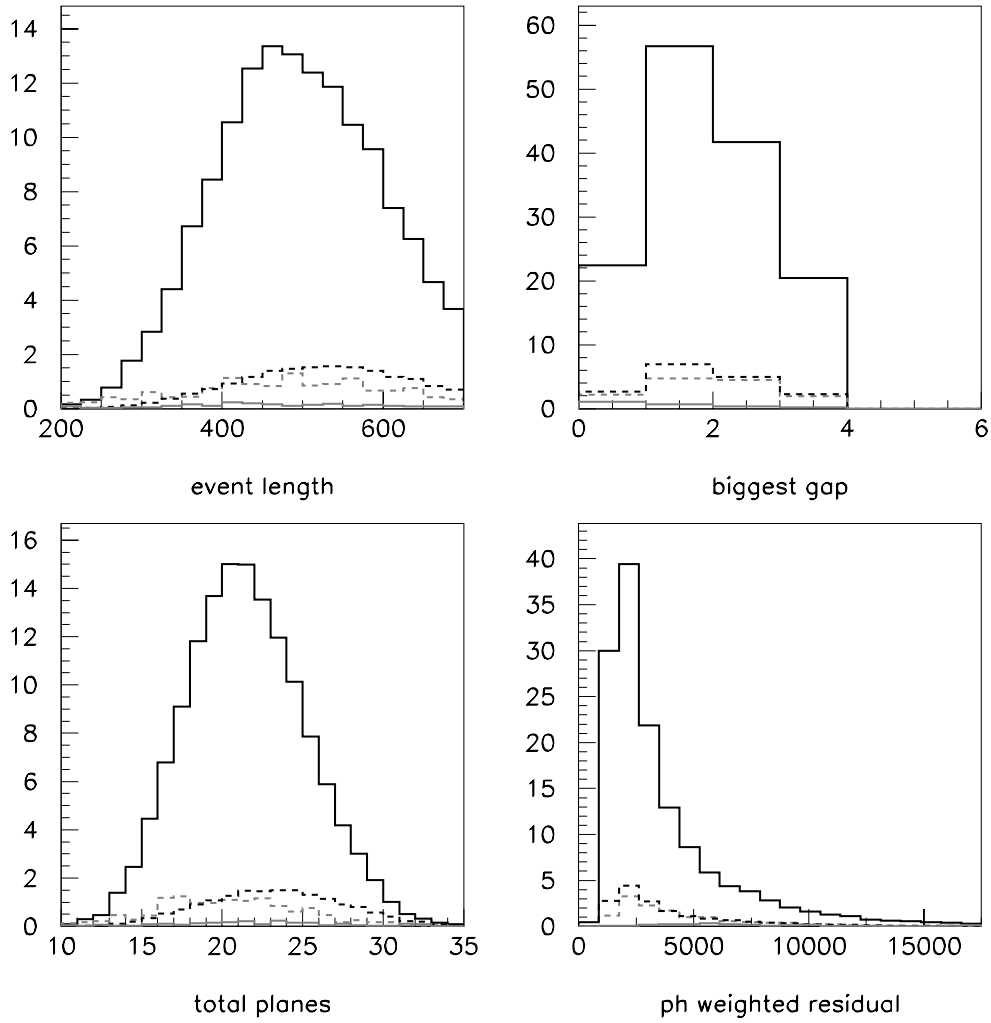


Figure 15 Distributions used in the likelihood function at 820km. Top left; the event length after the cuts. Top right; the largest gap (missed planes) in the event. Bottom left; the total number of hit planes in the event. Bottom right; the pulse height weighted residual to the straight line fitted to the event.

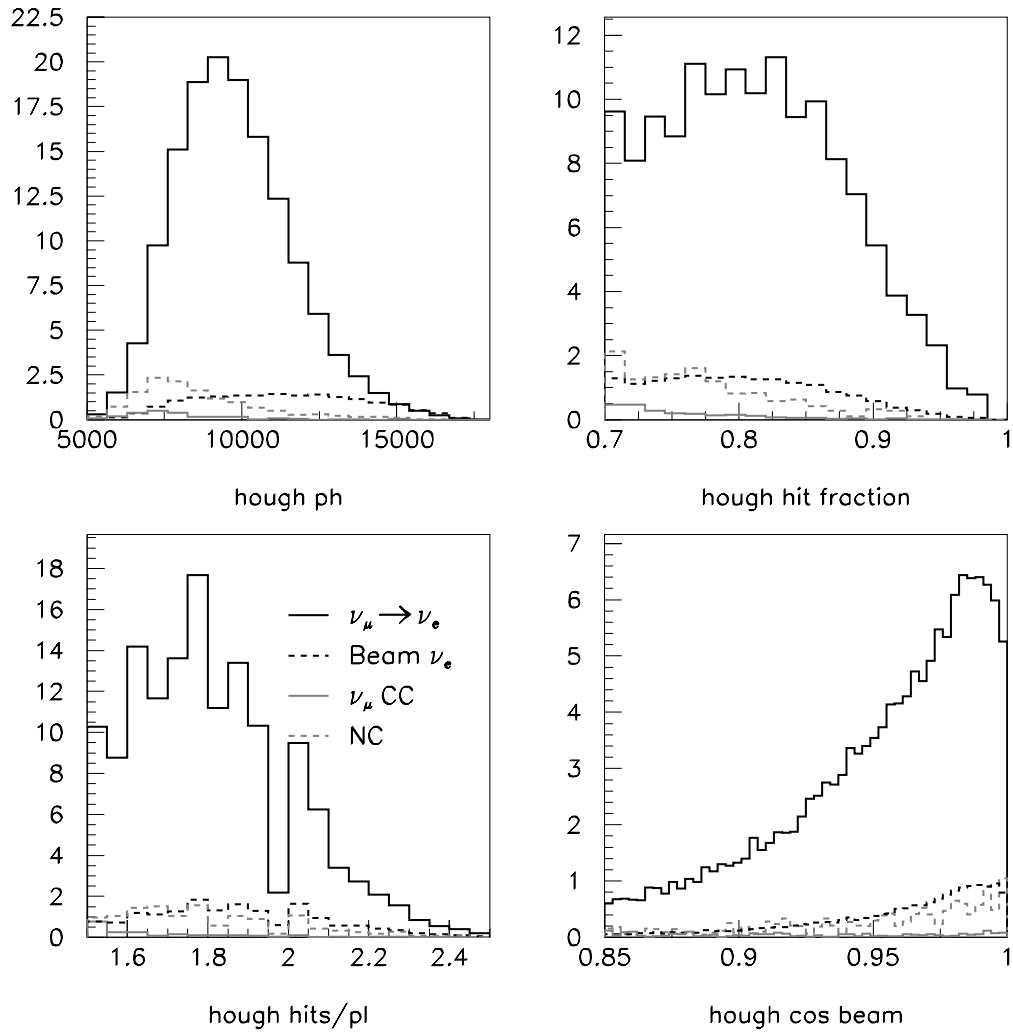


Figure 16 Distributions derived from hits selected by the Hough Transform (HT) filter at 820km. Top left: total pulse height. Top right: fraction of hits selected by HT filter over the total number of hits in the event. Bottom left: number of hits per plane. Bottom right: cosine of the angle between the straight line fit to the hits and the z axis.

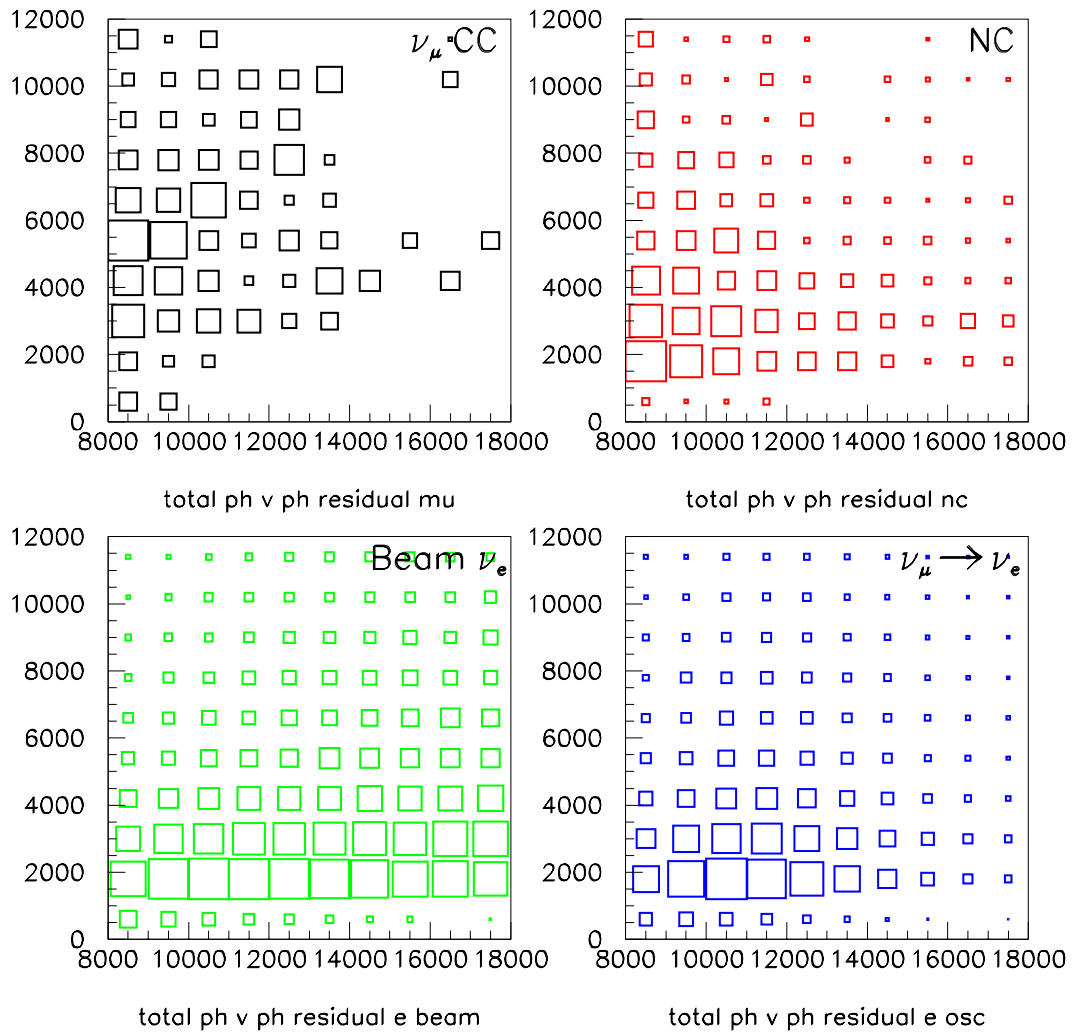


Figure 17 Total pulse height (x) versus pulse height residual (y) distributions for all hits in the four event classes at 820 km.

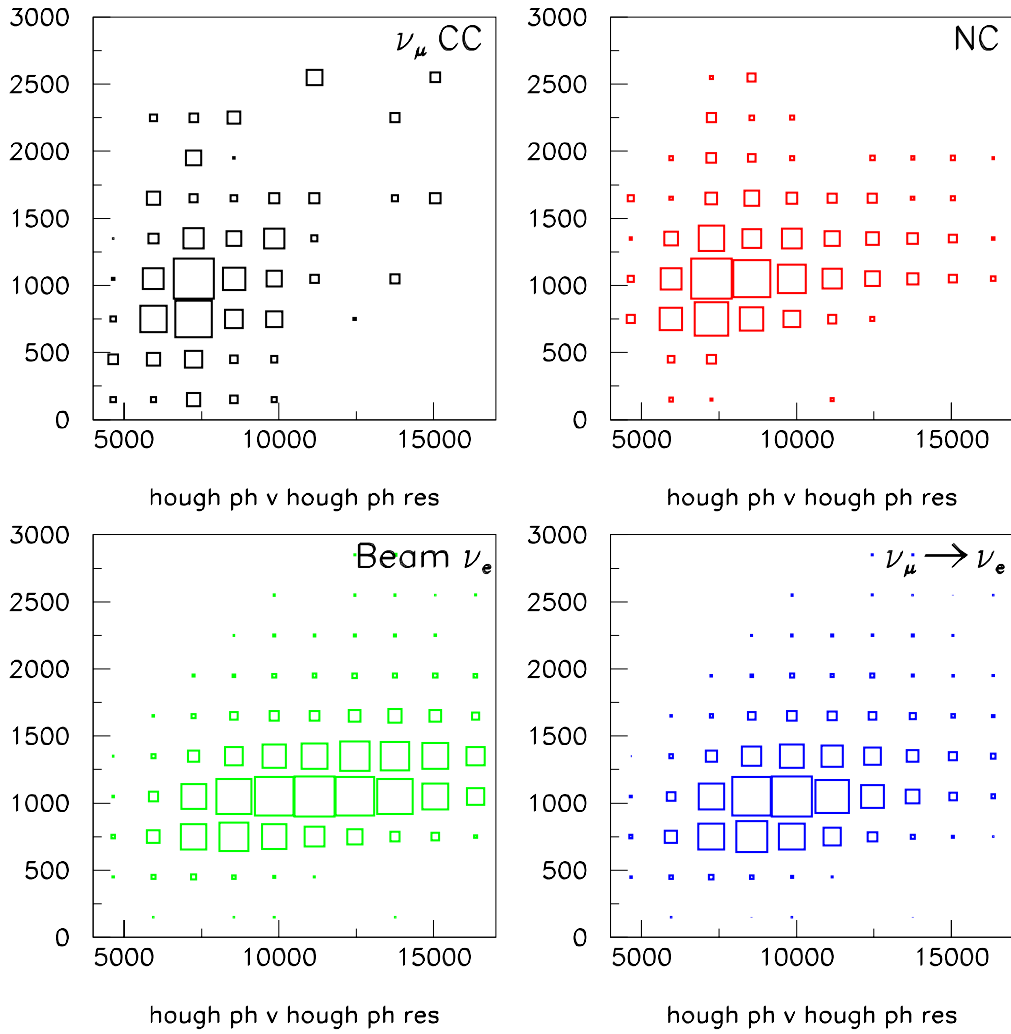


Figure 18 Total pulse height (x) versus pulse height residual (y) distributions from the hits assigned to the Hough track for the four event classes at 820km.

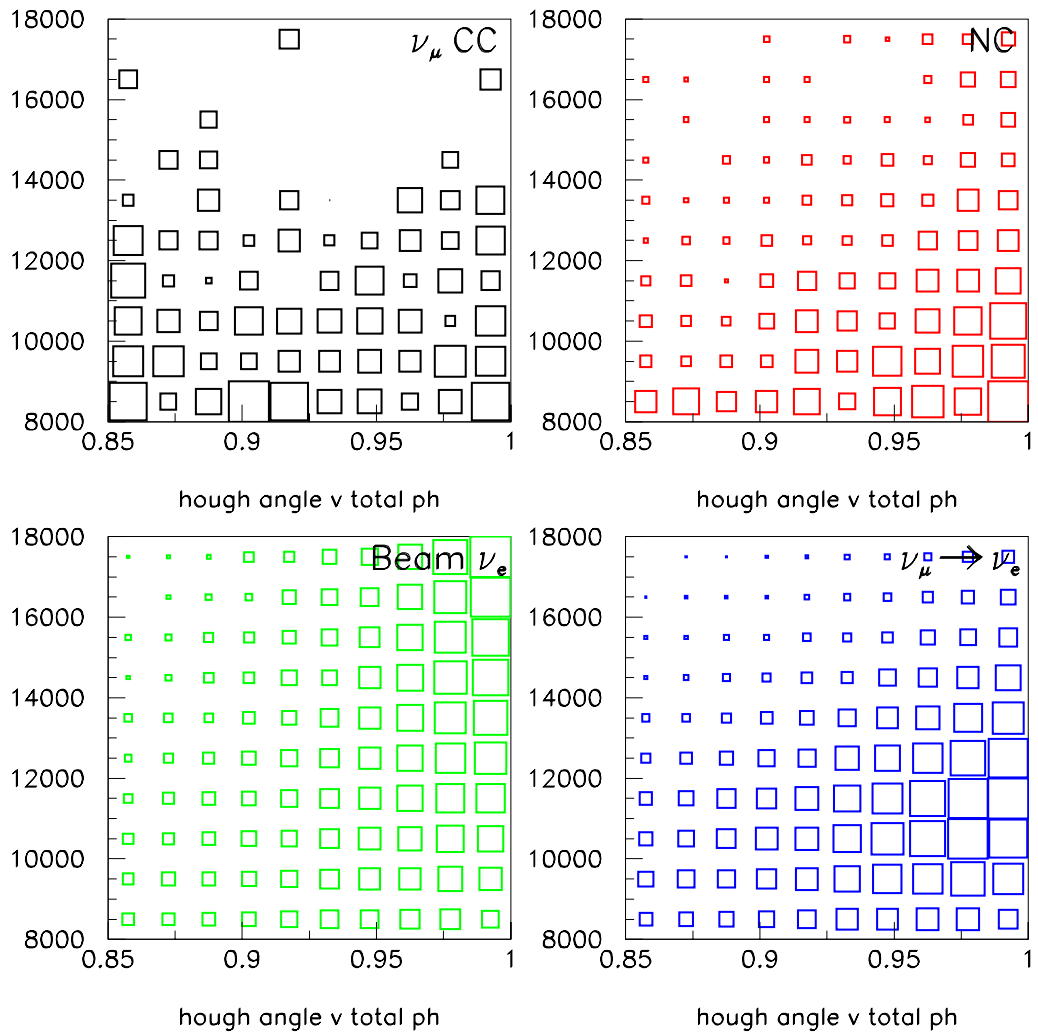


Figure 19 Cosine of the angle between the Hough track and the z axis (x) versus the total pulse height in the event (y) at 820km

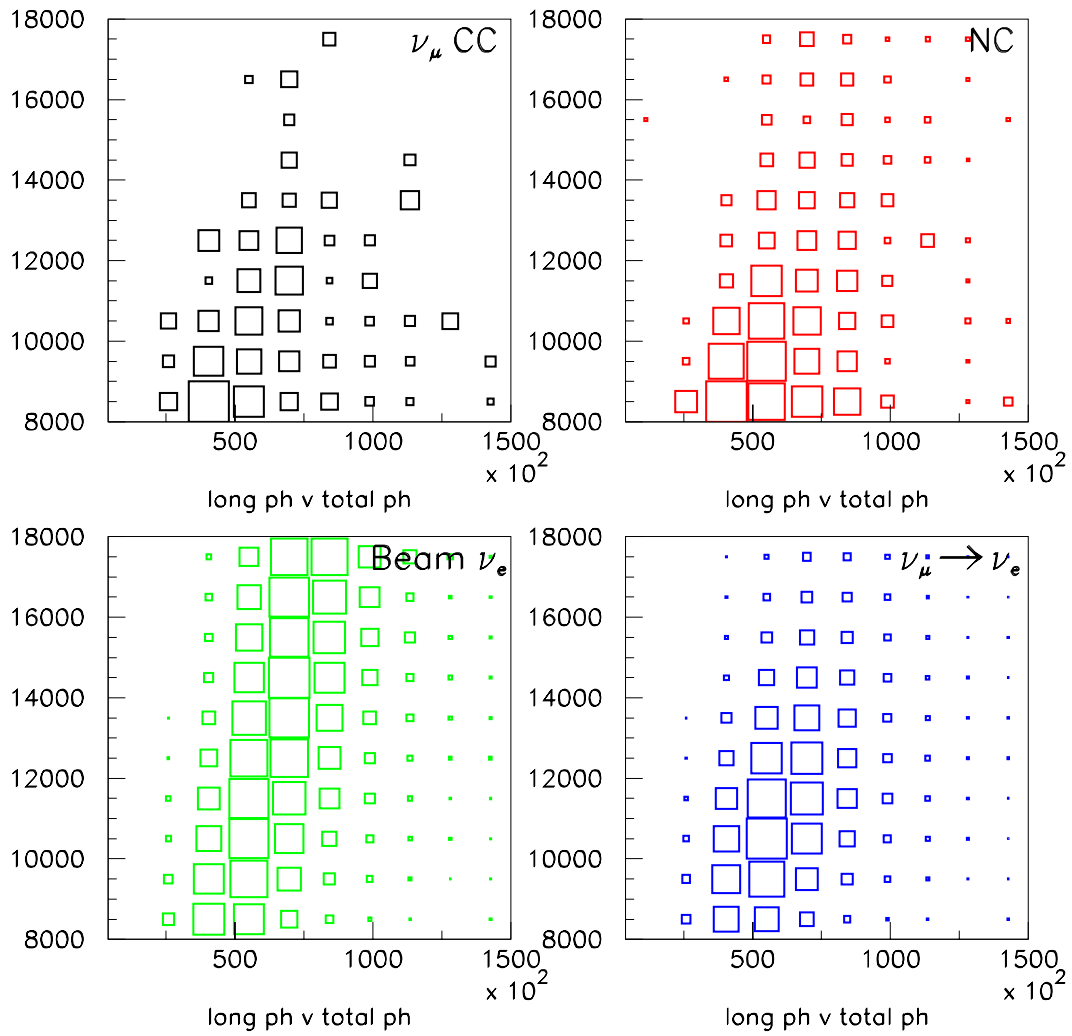


Figure 20 The rms of the pulse height times distance in the z direction (x) versus the total pulse height for hits in the total event (y) at 820 km

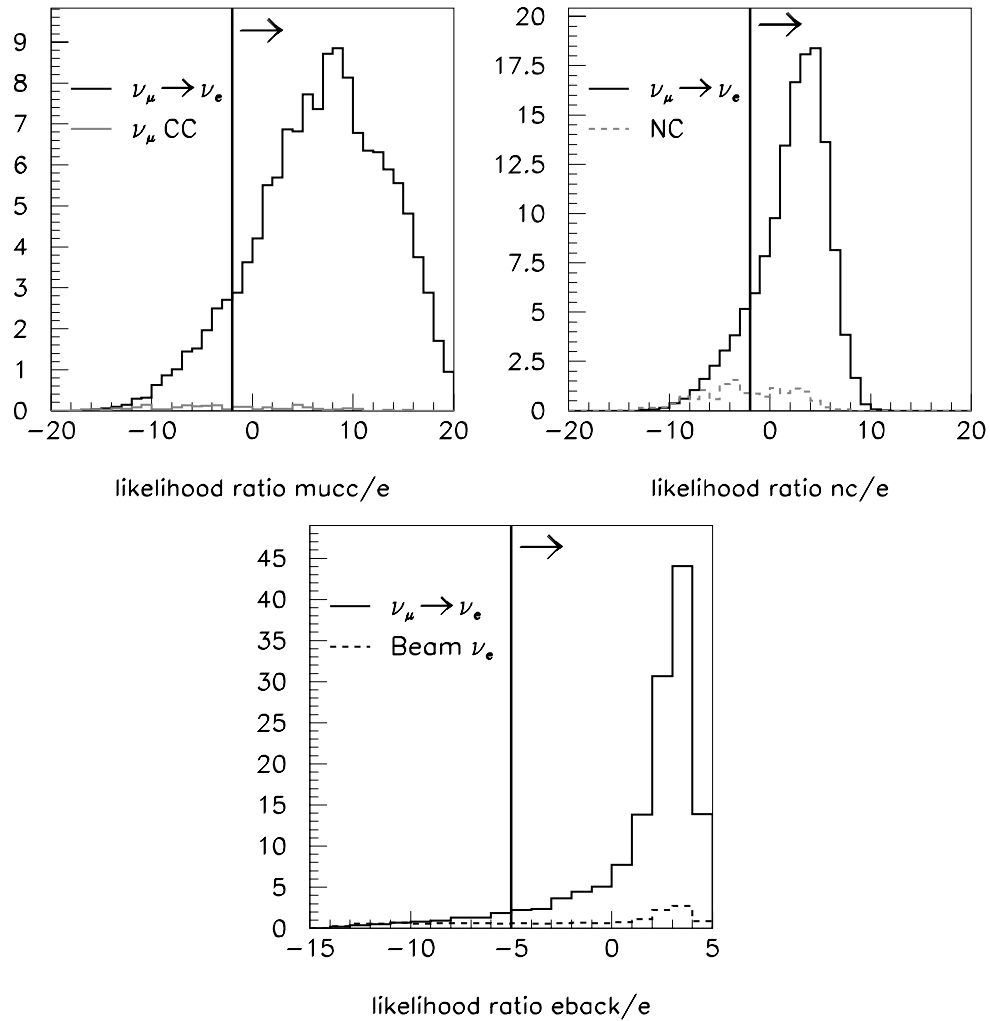


Figure 21 Log likelihood ratio distributions at 820km. Top left; log of the ratio of the ν_μ CC to the oscillated ν_e CC likelihood. Top right; log of the ratio of the NC to the oscillated ν_e CC likelihood. Bottom; log of the ratio of the beam ν_e CC to the oscillated ν_e CC likelihood.